Environmental Science
Water Research & Technology

ROYAL SOCIETY OF CHEMISTRY

PAPER

View Article Online
View Journal | View Issue

Cite this: *Environ. Sci.: Water Res. Technol.*, 2024, **10**, 2418

Innovations in water desalination: enhancing air gap membrane distillation performance by the incorporation of clay nanoparticles into PVDF matrix membranes†

Roberto Navarro-Tovar, [a] Patricia Gorgojo, [bc] Megan Jobson,[a] Peter Martin[a] and Maria Perez-Page *[a]

Received 21st April 2024,
Accepted 23rd July 2024

DOI: 10.1039/d4ew00326h

rsc.li/es-water

This study showcases the remarkable permeate flux rates achieved in water desalination using phase-inversion polyvinylidene difluoride (PVDF) membranes by the incorporation of clay nanoparticles within the polymer matrix, leading to a performance that surpasses that of commercial membranes. These findings hold promising implications for addressing water scarcity issues in various regions around the globe. The study focuses on membrane improvement by incorporating both montmorillonite (MT) and Cloisite 20A (organomontmorillonite, OMT). The permeate flux of the most effective OMT-enhanced membrane (with a 4 wt% loading) surpassed that of the commercial PVDF membrane by 12% and outperformed the pure PVDF membrane by 30% after a 24 hour testing period in air gap membrane distillation (AGMD), with rejection values exceeding 99.8%. Moreover, this membrane exhibited stability over 5 days of continuous testing, proving better performance than commercial PVDF membranes when exposed to a concentrated fouling humic acid solution. This fouling test experienced a 40% reduction in permeate flux compared to the 60% decline observed in the commercial PVDF membrane. These enhancements are attributed to increased surface porosity, higher liquid entry pressure, smaller mean pore size, and a uniform distribution of clay particles within the membrane matrix.

Water impact

This work provides a sustainable and efficient alternative solution to current technologies used in water desalination. We report remarkable permeate flux-rates and long-term stability in membrane distillation using novel PVDF/clay nanoparticle membranes. This achievement will lead to meeting the growing demand for clean water in regions that face critical water scarcity, one of the most important challenges in the 21st century.

1. Introduction

The availability of water for human consumption is rapidly declining due to widespread human activities. Freshwater scarcity is becoming a critical issue, particularly in arid regions, driving the need for practical solutions. Various desalination technologies, including multi-effect distillation, multi-stage flash, and membrane-based technologies, have been developed to address the growing water scarcity problem over recent decades. Notably, membrane technologies play a substantial role, contributing to approximately 68% of the total desalination capacity. This percentage is expected to rise steadily as the membrane market expands.[1]

Membrane distillation (MD) has brought increasing attention as an emerging technology suitable for treating seawater, brackish water, and industrial wastewater containing inorganic pollutants. This versatile MD system can be integrated with other separation processes, including nanofiltration (NF)[2] or reverse osmosis (RO) units,[3,4] creating a comprehensive and efficient separation system. Additionally, it is worth noting that MD technology exhibits the potential to employ renewable energy sources, as evidenced by its successful integration with solar energy,[5] and the use of waste heat from industrial processes.[6] In addition to its proficiency in desalination, MD is also highly efficient in extracting organic compounds and heavy metals from an extensive range of aqueous solutions.[7,8] Finally, it is worth highlighting that MD's

[a] *Department of Chemical Engineering, The University of Manchester, Manchester M13 9PL, UK. E-mail: maria.perez-page@manchester.ac.uk*
[b] *Instituto de Nanociencia y Materiales de Aragón (INMA), CSIC – Universidad de Zaragoza, Zaragoza, 50018, Spain*
[c] *Departamento de Ingeniería Química y Tecnologías del Medio Ambiente, Universidad de Zaragoza, Zaragoza, 50018, Spain*
† Electronic supplementary information (ESI) available. See DOI: https://doi.org/10.1039/d4ew00326h

adaptability extends beyond desalination, as it is also capable of addressing complex challenges such as the treatment of radioactive waste and ensuring the secure discharge of the treated product into the environment.[9]

MD operates as a thermally driven separation process grounded in the principles of liquid–vapor equilibrium. Operating non-isothermally, the process creates a temperature gradient across the membrane, which establishes a partial pressure gradient. This gradient causes volatile components to evaporate at the liquid–vapor interface near the membrane pores, allowing them to diffuse within the membrane. Air-gap MD (AGMD) offers distinct advantages over other MD arrangements among the different MD configurations. Unlike direct contact MD (DCMD), where both sides of the membrane are in direct contact with fluid, increasing the risk of membrane wetting, AGMD employs an air gap that significantly reduces this risk.[10] This air gap also minimises conductive heat losses, enhancing thermal efficiency. Compared to vacuum MD (VMD), where the applied vacuum can exacerbate membrane wetting, AGMD maintains a stable vapour–liquid interface, offering improved stability and performance.[11] The membrane must be both porous and hydrophobic to effectively prevent the passage of liquid water. Commercially available microporous hydrophobic membranes prepared from polymers, such as polytetrafluoroethylene (PTFE), polypropylene (PP), and polyvinylidene fluoride (PVDF), come in various forms (flat sheet, tubular, hollow fibre, and capillary) and are widely employed in laboratory MD experiments.[12] Muhamad *et al.*[10] reported the superiority of PVDF membranes in the MD process over PP or PTFE counterparts due to heightened mechanical and chemical stability, excellent processability, superior hydrophobicity, and heat resistance. In order to ensure that the most appropriate membrane is selected, it is essential to consider the scalability of membrane fabrication techniques. Nowadays, phase inversion has become the most prominent technique for membrane fabrication. It offers precise control over pore formation and membrane properties, and its scalability has enabled successful implementation in industrial production processes.[13] These techniques enable the efficient assembly of the membranes in modules on a large scale while considering the cost. The importance of this scalability factor cannot be overstated, particularly when we consider the widespread application of these membranes in water desalination processes.

Polymeric membranes in single layers encounter limitations, including low permeate flux, membrane wetting and fouling challenges. To address those challenges, composite membranes have been developed by the incorporation of inorganic fillers and 2D materials within the polymer matrix such as silica, titanium oxide, alumina, graphene oxide, metallic organic frameworks, or black phosphorus.[14–16] This strategy has proven effective in enhancing various membrane characteristics, such as selectivity, fouling resistance, and wetting reduction. Clay, a naturally occurring sedimentary material or soil, primarily comprises minerals from the phyllosilicate group. Several types of clay exist, including kaolinite, illite, smectite, and others. Smectites, which have a layered structure with basal spacing, allow for the intercalation of various molecules or polymers between the layers, thereby enabling the inclusion of polymer chains like PVDF that strengthen the bond between these materials.[17] Clays, particularly when incorporated into PVDF membranes, have garnered significant attention due to their high compatibility with polymers, abundance, and ability to enhance mechanical strength for improved long-term stability.[18] These composite membranes, containing clays like montmorillonite (MMT) and organoclays such as Cloisite 20A (OMT), offer benefits such as increased permeability, thermal resistance, abrasion resistance, and improved surface properties through robust interactions between polymer and clay.[19,20] Cloisite 20A, among other modified clays, stands out as a preferred nanofiller for MD composite membranes due to its high hydrophobicity, which is attributed to the significant amount of organic surfactant on the clay surface. This organically modified MMT, having dimethyl dehydrogenated tallow quaternary ammonium groups, ensures high hydrophobicity (Fig. S1†). This fundamental property guarantees membrane selectivity for vapour molecules and prevents issues like wetting and fouling in membrane distillation.

MMT has found wide-ranging applications in industry and research, particularly in catalytic,[21] electronic,[22] energy conversion,[23] and separation fields.[24] Its mechanical strength, heat resistance, adsorption capacity, and cost-effectiveness compared to other clay materials make it an attractive filler material for composite membranes in membrane applications.[25–27] While there has been limited literature on separation applications for MMT-based membranes, this area has recently gained attention.

Both MMT (hydrophilic) and Cloisite20A (hydrophobic) clays can be used as fillers for MD membranes due to their distinct surface properties. This implies that MMT has the potential to improve LEP and wetting resistance due to its hydrophilic nature. Conversely, the hydrophobic Cloisite20A is expected to enhance membrane hydrophobicity, thereby improving permeate flux and antifouling performance. This study compares these two fillers and investigates how hydrophilic and hydrophobic modifications impact overall membrane performance in membrane distillation applications.

In this work, phase inversion PVDF–clay mixed matrix membranes (MMMs) were successfully prepared using montmorillonite and Cloisite20A as fillers. The prepared membranes were evaluated to treat synthetic saline solutions *via* an air gap membrane distillation (AGMD) configuration. The PVDF–clay membranes underwent comprehensive analysis, including scanning electron microscopy, energy dispersive X-ray spectroscopy, contact angle, porosity, pore size/distribution, liquid entry pressure, and water permeate flux evaluation.

2. Experimental section

2.1 Materials

PVDF (MW = 534 000 g mol^{-1}) was purchased from Sigma Aldrich and was used to prepare the polymeric membranes. Dimethyl sulfoxide (DMSO, ≥99.5% pure) was purchased from Fisher Scientific UK and was used to dissolve the PVDF and prepare the dope solutions to fabricate the phase inversion membranes. Montmorillonite (MT) clay was purchased from Sigma Aldrich. Cloisite20A® (organomontmorillonite) (OMT) was obtained from Blagden UK. Sodium chloride (NaCl, ≥99.0%) was purchased from Merck and was used to produce artificial seawater. PVDF commercial membranes (GVHP09050) were purchased from Merck Life Science UK Limited. Humic acid (HA) was purchased from Merck Life Science Ltd and was used as organic foulant.

2.2 Membrane preparation

In order to prepare membrane dope solutions, PVDF was dissolved in DMSO containing either MT or OMT. The optimal concentration of PVDF (18 wt% of the total solution) was determined by assessing porosity, water contact angle and water flux of a range of membranes prepared from 13 to 20 wt% as shown in Fig. S2.† Dispersions of DMSO/MT or DMSO/OMT with varying concentrations (0.5, 2, 4, 6, and 8 wt% per total weight of PVDF) were prepared by adding 1.8 g of PVDF pellets to obtain a total solution weight of 10 g, as summarized in Table S1.† The dope solutions were vigorously stirred for 12 hours at 70 °C to ensure complete dissolution of the polymer. The solutions were allowed to rest for 2 h without agitation to facilitate degassing.

The membranes were synthesized using the non-solvent-induced phase inversion (NIPS) technique. Polypropylene non-woven support fabric sheets (Viledon Novatexx 2471) were affixed to glass plates and placed on an automatic film applicator (Sheen 1133 N). Subsequently, the dope solution was poured onto the support fabric and cast using an adjustable Sheen 1117 casting knife set at the height of 150 μm. Then, the glass plate was immediately submerged in a coagulation bath containing deionized (DI) water at 20 °C. Following a 10 minute immersion, the glass plate was transferred to a separate DI water bath for 24 h. Subsequently, the membranes were removed from the water bath and allowed to dry overnight.

Membrane codes were used as follows: CM stands for commercial PVDF, PR for pristine PVDF, and the upper numbers of MT and OMT stands for the concentration loadings.

2.3 Characterization of materials and membranes

The morphological analysis of the membranes was conducted utilizing a scanning electron microscope (SEM) Quanta FEI 250, USA. Cryogenic fracturing with liquid nitrogen of ethanol pre-wetted membrane samples was employed to obtain cross-sections. The microscope was equipped with Energy Dispersive X-ray Spectroscopy (EDX), which was used to identify and give approximate measures of the content of Si and Al elements present in the membranes. To prepare the samples for imaging, a thin layer of 5 nm of gold/palladium (Au/Pd 80/20) was sputter-coated on all samples using a Q150R – rotary pumped coater, Quorum, UK.

An optical tensiometer, Attention Theta from Biolin Scientific, UK, was used to measure water contact angle (CA). The CA values were meticulously measured at 5 second intervals from when the droplet came into contact with the membrane surface until 30 s. The experiment was carried out three times for each sample, and the values reported are the averages.

A dead-end filtration cell manufactured by Sterlitech, USA, was used to determine liquid entry pressure (LEP) values. The filtration cell was initially filled with 200 mL of an aqueous solution containing 35 g L^{-1} of NaCl. Gradually, pressure was applied on the feed side until permeate liquid appeared on the permeate side, indicating that the LEP had been reached. The pressure at this point was recorded as the LEP value. The average of three experiment repetitions was reported.

To determine the thickness of the membranes, a digital micrometer screw gauge was employed, with a precision of ±0.5 μm (Mitutoyo IP65 Coolant Proof, Japan). More than five measurements were taken for each sample, and the values reported are the averages.

The porosity of the membranes was determined through the gravimetric method and calculated using eqn (1):

$$\varepsilon = \frac{\frac{W_W - W_d}{\rho_l}}{\frac{W_W - W_d}{\rho_l} + \frac{W_d}{\rho_p}} \quad (1)$$

where, W_W and W_d are the weight of wet and dry membrane, respectively. ρ_l and ρ_p are densities of ethanol (789 kg m^{-3}) and PVDF polymer (1740 kg m^{-3}).[28,29] The membranes were immersed in ethanol for 30 seconds, carefully wiped out with a paper towel to remove excess liquid, and immediately weighed. The values reported correspond to the average of five repeated measurements.

Capillary flow porometry (CFP) was utilized to perform an in-depth analysis of the pore structure of the manufactured membranes. A Porolux 1000 porometer, manufactured by Porometer, Belgium, was employed to obtain automatic measurements of the bubble point, mean flow pore (MFP) size, smallest pore size, and pore size distribution using the wet/dry method. Initially, membrane samples of 2.98 cm^2 were submerged in Porefil 125, a specialized pore-filling liquid sourced from Porolux, for five seconds. Nitrogen (N_2) was then applied to exert pressure and displace the liquid from the pores. This allowed for measuring gas flow against the applied pressure and constructing a "wet curve". Finally, pressure was applied to the dry sample to obtain a "dry curve". The pore size was calculated using eqn (2):

$$P = \frac{4\gamma \cos\theta}{D} \quad (2)$$

where, P is the pressure required to displace the wetting liquid from the pore, D is the pore diameter, γ the surface tension of the wetting liquid (15.88 ± 0.03 mN m^{-1} (ref. 30)) and θ the contact angle of the wetting liquid. The result was obtained as the average of three measurements.

2.4 Membrane distillation performance

Desalination experiments were conducted using an AGMD system during 24 h of continuous operation. The feed solution (35 g L^{-1} of NaCl) was efficiently circulated through the membrane module utilizing a 12 V pump at a constant rate of 1 L min^{-1}. Temperature regulation for the cooling fluid (20 °C) was achieved by using a Julabo F12-ED chiller, which circulated DI water to the module at a rate of 0.6 L min^{-1}. The membrane module, which had an air gap of 3 mm and an effective area of 7.6 cm^2, facilitated the exit of permeate vapour through gravity and collection in a measuring cylinder. For each experiment, the permeate beaker was filled with 100 mL of DI water, and the conductivity was accurately measured using a digital conductivity meter (GO Direct Conductivity Probe, UK). Additionally, a precise weight change measurement was recorded over time using a precision weigh scale (HCB 6001, Adam Equipment, UK). A minimum of three membranes were tested and average permeate flux and salt rejection values are reported. A diagram of the AGMD laboratory system is illustrated in Fig. 1.

Determination of permeate flux (J_{exp}, kg m^{-2} h^{-1}) in MD is essential. To calculate this parameter eqn (3) was employed, which takes into account variables such as the change in the permeate mass beaker (Δm, kg), the effective membrane area (A_m, m^2), and the sampling period (Δt, h).

$$J_{exp} = \frac{\Delta m}{(\Delta t)A_m} \quad (3)$$

Moreover, the salt rejection (SR, %) is another critical parameter to evaluate the suitability of a membrane for MD. This parameter was calculated using eqn (4):

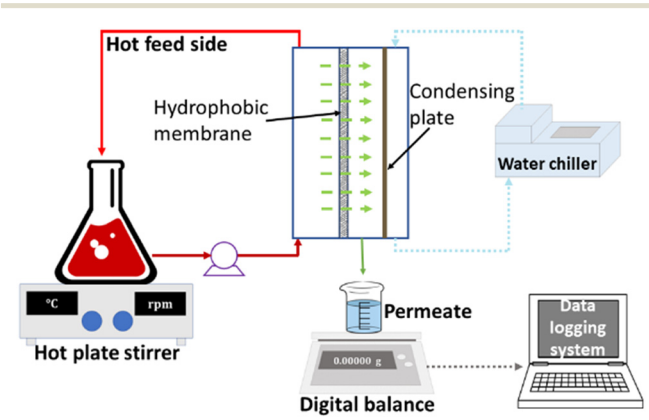

Fig. 1 Schematic diagram of the experimental rig of the AGMD process.

$$SR = \left(1 - \frac{C_p}{C_f}\right) \times 100 \quad (4)$$

where C_p and C_f are the concentration of the permeate and concentration of the feed, respectively.

In order to evaluate the phenomenon of organic fouling, additional experiments with humic acid were conducted, where saline solutions initially contained 100 ppm of HA. The reason behind selecting HA was because natural organic matter (NOM), primarily composed of humic substances, is present in surface waters and serves as the primary precursor of scaling in MD membranes.

3. Results and discussion

3.1 Membrane characterization

To evaluate the morphology of the membranes, SEM and EDX were carried out for the clay material surface and cross-section of the membranes. Fig. 2b and c shows the membranes surface micrographs for the PVDF with MT and OMT particles. It is worth to mention that the MMM SEM images displayed in Fig. 2, correspond to a 4% clay loading, which is the optimal loading, which is the optimal loading, based on the results obtained for different critical parameters (LEP, CA, porosity, permeate flux, salt rejection and cost), which is presented in the following sections. Both images exhibit the presence of clay particles on the surface of the composite membrane as clustered (bright-white) dots with a particle size of approximately 1–3 μm. The SEM surface images suggest that the clay particles are well dispersed on the membrane's inner surface without significant agglomeration. Most clays' reported original particle size is less than 3 μm,[31] which agrees with the dot particles seen on the surface SEM images and in Fig. S3.†

Fig. 2d–f and S4† show the cross-sections of the membranes with an asymmetric porous structure. The morphologies illustrate a sponge-like layer in contact with the permeate side on the upper side of the image, followed by finger-like macropores and a thin microporous layer in contact with the feed solution, serving as a selective layer to allow only vapour to pass through. Although adding clay particles did not markedly alter the proportion of macrovoids, it induced changes in the pore structure, resulting in more extensive and more uniformly distributed pores, as shown in Fig. 2f for the MMMs of OMT. This modification occurred because clay particles act as nucleation sites for pore formation, facilitating a more controlled and uniform distribution of pores throughout the membrane.[32,33] However, for the MT clay particles can lead to wider macrovoids, as it is shown in Fig. 2e. This is due to the hydrophilic nature of the MT that could promote faster demixing rates subsequently forming large macrovoids in the membrane structure.[34]

According to the results obtained from the EDX analysis, as presented in Table S2† and visually depicted in Fig. 3 and S5,† the presence of clay particles is confirmed in the

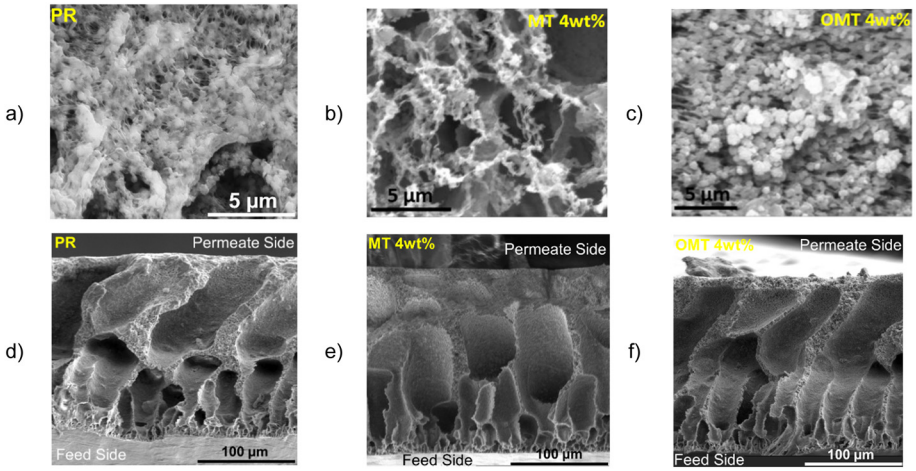

Fig. 2 Surface SEM images (magnification ×8500) of a) pristine PVDF, and MMMs having b) 4 wt% of MT, and c) 4 wt% of OMT; and membrane cross-sections (magnification ×600) of d) pristine PVDF, and MMMs of e) MT and f) OMT at 4 wt% both of each.

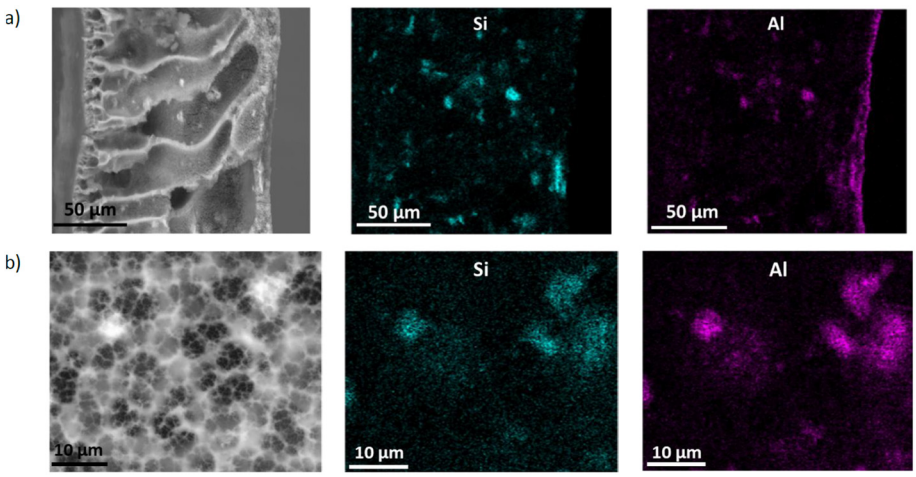

Fig. 3 EDX mapping of Si (center side) and Al (right side) elements for the a) cross-section and b) surface micrographs of PVDF–OMT 4 wt% membrane.

manufactured membranes. The analysis further demonstrated the detection of silicon (Si) and aluminium (Al) on the membrane surface, with Si being the most predominant element. The concentration of these elements, especially Si, increases with the clay loading in the membrane. A positive correlation between high Si contain into the membranes is observed, leading to increasing membrane porosity and hydrophobicity, which are key factors to enhance the effectiveness of membranes in MD.[33] Furthermore, the presence of a clear line of Al element at the top surface has been observed, suggesting that Al-containing compounds in the OMT tend to concentrate on the surface during the phase inversion process. This accumulation may be due to the interaction between the PVDF polymer matrix and clay particles, causing the particles to move towards the surface during solidification.[35,36] In contrast, the Si element is distributed evenly throughout the membrane, indicating a more uniform dispersion of Si-containing compounds within the clay. This uniform distribution is likely due to the nanoscale dispersion of silica particles and their compatibility with the PVDF matrix, which allows for even incorporation during membrane casting and solidification.[37]

The porosity and pore size of each membrane has been measured, and the results are displayed in Fig. 4a and b.

MD membrane porosity generally lies between 65 and 85%.[38] In this study, the porosity of all samples ranged between 74% and 86%, which is advantageous because high porosity values have a larger surface area leading to enhance of vapour transport through the membrane. When MT was added to the membrane, the resulting porosity values were around 75%. This could be attributed to the hydrophilic nature of the material, which may cause a faster solvent exchange during the membrane formation process, leading to bigger macrovoid pores. However, the incorporation of OMT clay material yields a porosity level that surpasses 80%. The high porosity is attributed to the hydrophobicity of the material and the contribution of

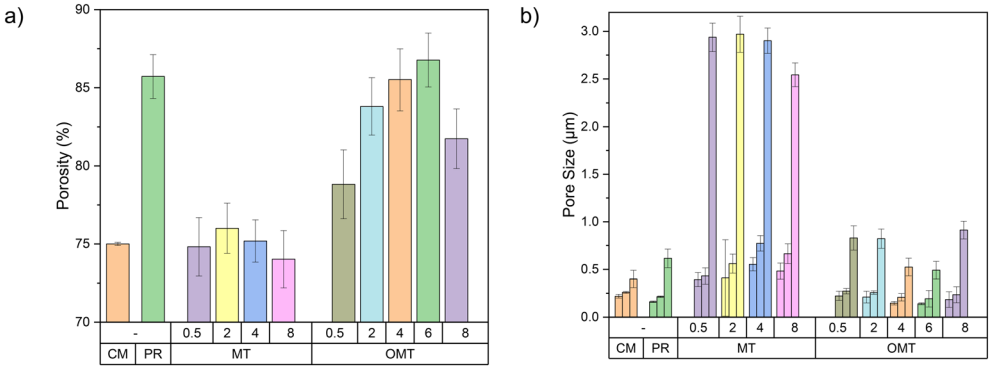

Fig. 4 a) porosity, and b) pore size of all fabricated PVDF–clay membranes. From left to right, the bars indicated the smallest, mean and largest pore size obtained. Error bars represent standard deviations from three samples (or five in the case of the porosity). CM stands for commercial PVDF, PR for pristine PVDF, and the upper numbers of MT and OMT stands for the concentration loadings. Due to the similarity of results obtained for the MT material, only 0.5, 4, and 8 wt% have been displayed to avoid a visual pileup of results.

DMSO. The modified clay material exhibits hydrophobic properties, thereby inducing a thermodynamic immiscibility within the dope solution. This effect accelerates the exchange between the solvent and non-solvent components, facilitating the formation of a porous structure.[39] The larger Hansen solubility parameters between PVDF and DMSO (total solubility δ_T = 24.2, dispersion forces component δ_d = 17.2, polar force component δ_p = 12.5, hydrogen bonding component δ_h = 9.2, and δ_T = 26.7, δ_d = 18.4, δ_p = 16.4, δ_h = 10.2 MPa, respectively)[40] and the lower diffusion rate of DMSO and water,[41] allow for immediate phase separation when the casting solution comes in contact with the coagulation bath and solidification is postponed. This leads to the formation of a porous top layer acting as selective barrier, and the complete development of macrovoids in the sub-layer, structure that can be observed in the SEM images presented previously (Fig. 2c–e).[40,42] The large internal pores observed in cross-sectional SEM images, also account for the high porosity of PVDF-related membranes.

The mean pore size changes observed in the PVDF–clay membranes align with the porosity changes. The hydrophilic properties of the MT material accelerate the demixing rates, which results in larger pores. On the other hand, the hydrophobic nature of the OMT can enhance the demixing process, leading to more controlled pore size and distribution as the pristine membranes. As the OMT loading increases beyond 0.5 wt% at the same time as the dope solution viscosity, the mean pore size of the PVDF–OMT membranes decreases. At 6 wt% of OMT, the mean pore size decreases to 193 nm. This reduction can be attributed to the higher viscosity in the dope solution at higher clay loadings, which results in slower and more controlled solvent–nonsolvent exchange,[43] leading to smaller pore sizes, as shown in Fig. 4b. Nevertheless, a sudden increase in the pore size of OMT8 has been observed. According to the pore size distribution analysis (Fig. S7†), this indicates a shift towards the larger pores region in the OMT8 membrane, suggesting a larger quantity of larger pores than membranes with lower OMT loadings. The unexpected increase in pore size for the OMT 8 wt% membrane can be attributed to the overloading of clay nanoparticles, which likely leads to agglomeration. Clay nanoparticles are well-dispersed at lower concentrations within the PVDF matrix, effectively creating a uniform network that helps reduce pore size. However, due to van der Waals forces, the excess nanoparticles tend to cluster together at higher concentrations, such as 8 wt%.[44] This clustering can disrupt the membrane structure's uniformity, resulting in the formation of larger pores. Moreover, excessive clay particles may hinder the polymer chain entanglement, which is crucial for forming a dense and uniform membrane structure. The compromised entanglement can create voids and larger pores as the polymer matrix cannot wholly encapsulate the excessive clay particles. Finally, larger pores in MD membranes lead to lower LEP, increasing the risk of pore wetting, where the feed solution penetrates and wets the membrane, compromising the membrane's selectivity, permitting the passage of unwanted contaminants and reducing the purity of the permeate.

To evaluate the membranes hydrophobicity, water contact angle was measured for all of them. To be classified as hydrophobic, the membrane contact angle must be greater than 90°; otherwise, it is classified as a hydrophilic material. Fig. 5a shows the contact angle results obtained. The pristine PVDF membrane exhibited a value of 91.8°, whereas the commercial PVDF membrane demonstrated the highest value of 131.9°. This could be explained by the commercial PVDF membrane's symmetric structure and uniform composition throughout, as shown in Fig. S8.† This results in fewer sites with air pocket formation, leading to the highest contact area with an applied water droplet and increasing contact angle hysteresis.[45] The addition of natural montmorillonite resulted in contact angle values below 90°. This is because montmorillonite is inherently hydrophilic, presenting hydroxyl groups on its surface. This leads to a strong attraction to water molecules and swelling behaviour in the presence of water. However, there was a slight increase in the contact angle, from 69.4° for MT0.5 to 73.8° for MT8, as the MT loading increased. This increase can be attributed to changes in membrane surface roughness when MT particles were added. An increase in surface roughness can suggest

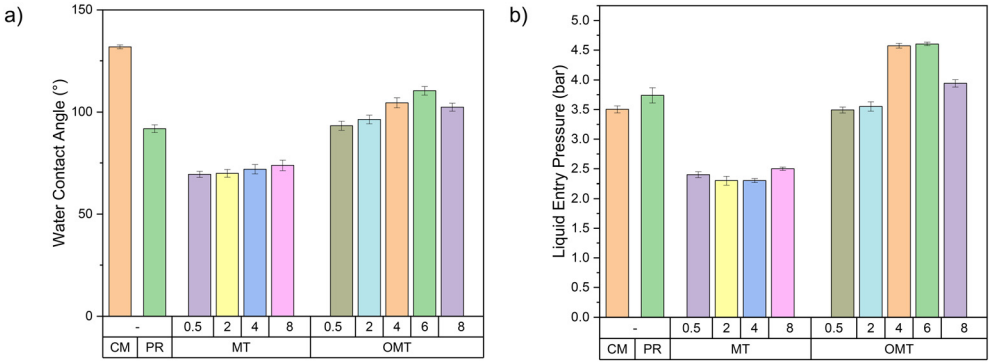

Fig. 5 a) Water CA and b) LEP of fabricated PVDF–clay membranes. Error bars represent standard deviations from three samples.

the apparent contact angle to increase, even if the material's actual contact angle should decrease.[46] The Wenzel and Cassie–Baxter models can describe this phenomenon.[47] In addition, at higher MT loadings, the distribution of clay particles may become less uniform, leading to localised regions where the hydrophilic MT is less exposed on the membrane surface. This uneven distribution can result in the membrane's overall hydrophobicity being slightly higher than expected. Furthermore, the agglomeration of MT particles at higher loadings can reduce the effective surface area of the hydrophilic clay exposed to water, thus causing a slight increase in the contact angle.

Otherwise, it can be observed that the addition of OMT clay particles to fabricated membranes results in an increased contact angle. This is primarily due to the use of organic surfactants, which modify MT into OMT and effectively shield the hydroxyl groups on the surface of montmorillonite, replacing them with hydrophobic organic chains. In addition, high porosity and smaller pore sizes are another parameter that can contribute to the increased contact angle. Recent studies have revealed that this phenomenon is attributable to the higher surface roughness of the membranes, which creates air pockets beneath the rough surface. This effect is named The Wenzel or Cassie effect, and explains that the air pockets hinder liquid from penetrating the grooves, leading to an increase in the water contact angle.[47] This effect could explain the observed behaviour for the OMT membranes developed in our work, providing a more hydrophobic behavior for the ones with higher porosity and lower pore size. At a concentration of 6 wt% of OMT, a contact angle value of 110.5° was obtained, more than 18° higher than the pristine PVDF membrane. This demonstrates that adding clay particles can enhance the surface hydrophobicity of membranes with appropriate hydrophobic modifications. Based on the characterization analysis, it is suggested that a concentration of 6 wt% of OMT would be an ideal loading for producing membranes for membrane distillation. However, the analysis also showed that using 4 wt% of OMT could produce similar results, making it another potential option for the optimal concentration, due to a more cost-effective since the raw material costs would be lower.

The average liquid entry pressure for all PVDF–clay membranes is shown in Fig. 5b. Composite membranes exhibit higher LEP values that suggest an ability to prevent liquid penetration through membrane pores, even in scenarios where there is a pressure difference between the feed and permeate sides. As a result, membranes with higher LEP offer enhanced performance, stability, and reliability in MD applications, especially when faced with varying operational pressures and temperatures. This characteristic is fundamental in preserving the membrane's desired separation efficiency and operational longevity. LEP results demonstrate comparable behaviour to contact angle values. Adding natural MT to the membranes resulted in the lowest LEP values. This is because MT is a hydrophilic material that increases the membrane's affinity for liquids, especially water. This enhanced hydrophilicity reduces LEP, making the membrane more susceptible to liquid intrusion at lower pressures. In contrast, LEP increases as the clay concentration increases for PVDF–OMT membranes. At the highest OMT concentration of 8 wt%, the membrane exhibits an LEP of 3.94 ± 0.06 bar. The decrease in the LEP for the OMT8 membrane is associated with the changes in pore size distribution, as indicated in our data (Fig. S7†). As previously mentioned, the pore size distribution for the OMT8 membrane demonstrates a shift towards larger pore sizes. According to principles of membrane distillation, higher LEP values are typically correlated with smaller pore sizes due to the more significant pressure required for liquid to permeate. The increase in pore size at higher OMT loading results in a lower LEP value, aligning with the observed data.

For 4 and 6 wt% concentrations, the LEP values are 4.57 ± 0.04 and 4.60 ± 0.03 bar, respectively. As previously discussed, the smaller pore sizes (0.14 μm) and higher porosity (87%) for these concentrations account for these results.

Table S3† summarizes the different properties evaluated for each membrane in comparison with the PVDF commercial membrane and the flux values. Membranes containing OMT exhibit higher liquid entry pressure and porosity values than commercially available PVDF membranes. At 4 and 6 wt% loadings, OMT displays smaller pore sizes, indicating a significant advantage in terms of antiwetting properties. In addition, OMT membranes exhibit notable contact angle

values. All previous characteristics indicate their potential for achieving higher permeate flux values.

3.2 Membrane performance within AGMD set-up

The incorporation of the clay materials within the polymer matrix has a clear effect on the membranes morphology, as it has been discussed in previous sections. This modification on the structure led to an enhancement of specific properties, which will have an impact on the membrane's performance in the desalination process. To evaluate this impact, PVDF–clay membranes were tested in the AGMD setup. Permeate flux and salt rejection are the main parameters to define the performance of the AGMD. A feed salt solution with a concentration of 35 g L^{-1} of NaCl, was prepared for each experiment to mimic the concentration present in the seawater.[48] Fig. 6a shows the AGMD average total permeate flux of the composite membranes at a feed temperature of 60 °C. Even though higher temperatures generally lead to greater permeate flux (Fig. 6b), operating at excessively high temperatures can cause issues related to material compatibility, leading to the degradation of the membrane and other components. Furthermore, selecting this temperature aligns with energy efficiency goals since maintaining high temperatures requires more energy input, eventually affecting the process's economic viability. Safety is a top priority, and a temperature of 60 °C ensures a safe experimental setup without compromising the output results. The study findings reveal a noteworthy influence of clay particles within the membrane on the permeate flux. The addition of montmorillonite clay in its natural form leads to lower permeate flux values, which is due to the fact that MT is a hydrophilic material that can absorb water and swell, leading to pore blockage at the start of the membrane distillation operation. Furthermore, the hydrophilic properties of MT cause the membrane to become wet very quickly. According to Fig. S9,† the membrane becomes wet within 2 to 4 hours, leading to the passage of salt particles and contaminating the permeate. This rapid wetting significantly reduces the membrane's effectiveness and discourage the use of natural MT in membrane distillation applications. From the characteristics described above for the MT clay, it is predicted that the modified material (OMT) will improve its hydrophobicity producing better permeate flow results because this modification forms a stable coating that shields the hydroxyl groups on the surface of the montmorillonite that causes the hydrophilic behavior of the material. This was confirmed by the higher permeate values of the PVDF–OMT membranes at 2, 4, 6, and 8 wt% concentrations as compared to those for all the manufactured membranes, even above the commercial PVDF membrane, obtaining an optimal concentration of 4 wt% (8.6 ± 0.3 kg m^{-2} h^{-1}). Salt rejection (values are plotted in Fig. 6a) was maintained above 99.8% at all time in all experiments. OMT4 was found as the optimal concentration among OMT materials due to its higher permeate flux, improved values of liquid entry pressure, and smaller pore size. Moreover, its economic advantage, with a lower weight concentration of the filler (4% compared to OMT 6%), makes OMT4 a cost-effective (~1.5 USD$ per kg of MT *vs.* 1.6 USD$ per kg of OMT[31,49]) and efficient option for MD applications.

The effect of the temperature on the desalination performance was evaluated for the optimal membrane PVDF–OMT 4 wt% and the commercial PVDF. Fig. 6b shows the AGMD average total permeate flux at different temperatures, where it can be observed that an increase in the feed temperature significantly enhanced the permeate flux. This is attributed to increased feed side membrane surface temperature, raising the driving force and the partial vapour pressure gradient. However, incorporating hydrophobic filler materials can further enhance this process by preventing membrane wetting, improving thermal stability, and increasing mechanical strength. Additionally, the membrane's reduced surface energy decreases interactions with water molecules, which collectively optimizes water vapour transport. All of these attributes work together with the thermodynamic effects of temperature, resulting in a more comprehensive increase in permeate flux. On these results, raising the temperature from 60 to 80 °C for the OMT 4 wt% increases the permeate flux by 165% (from 8.6 to

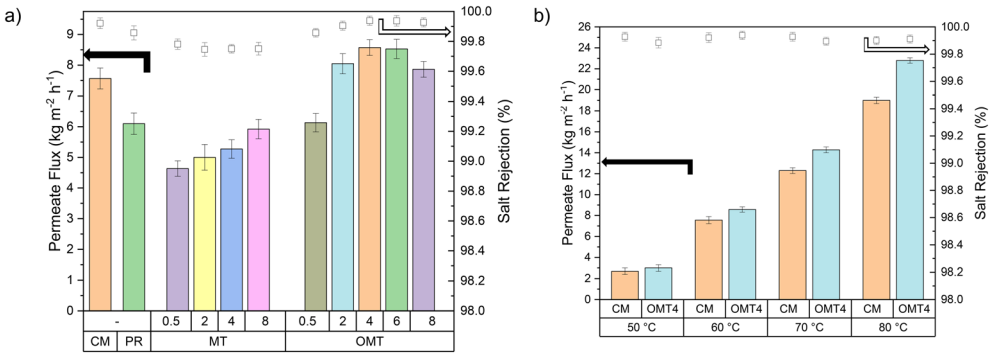

Fig. 6 Average total permeate flux and salt rejection of the prepared PVDF–clay membranes at a) 60 °C and at b) different feed temperatures for commercial PVDF and the OMT 4 wt% membranes. Columns: permeate flux (kg m^{-2} h^{-1}), and square symbols □: salt rejection (%). Error bars represent standard deviations from three samples.

22.8 kg m^{-2} h^{-1}). At higher temperatures, the changes in vapour pressure are not proportional to the temperature increments. This relationship can be described using the Clausius–Clapeyron eqn (S1),† which shows an exponential connection between temperature and saturation vapour pressure. Due to the inverse exponential term in the equation, even small increments in temperature can lead to significantly more significant changes in vapour pressure. This non-linear relationship, combined with a more substantial vapour pressure difference and increased molecular kinetic energy, results in a pronounced and exponential increase in permeate flux. The temperature's impact on vaporization becomes more significant, particularly at elevated temperatures, driving enhanced efficiency in membrane distillation processes.[50]

OMT4 not only exhibits a higher flux but also demonstrates consistent stability and effectiveness across a range of temperatures, hence confirming its robustness and reliability in various operational conditions.

3.3 Stability test

As discussed, an optimal PVDF–clay membrane material was found for the organomontmorillonite (OMT4) at 4 wt%. This membrane was tested to evaluate the longer-term stability and the antifouling properties. Long-term tests were carried out, operating the membrane for five days and maintaining the permeate flux and salt rejection at desired levels. Once the membrane could operate at good salt rejection values, fouling experiments were evaluated. Fresh membranes were tested with the addition of foulant agents into the feed solution to address the technical challenges of fouling phenomena that limit the practical applications of MD on a large scale. Fouling is the phenomenon where either inorganic or organic matter accumulates on the surface of a membrane. It can manifest in different forms, including partial or total fouling, where the pores become obstructed, decreasing the permeate flux rate.[51] Additionally, fouling can lead to pore wetting, resulting in considerably increased permeate flux. It is important to note that MD can only be performed using hydrophobic porous membranes, meaning the membrane's pores must not get wet by the liquid feed.

The long-term performance stability of the commercial PVDF and OMT4 membranes were evaluated for five days. The results shown in Fig. 7a, indicate that both membranes maintain a high rejection rate of over 99.8% while a permeate flux of 7.0 and 8.1 kg m^{-2} h^{-1} for the commercial and OMT4, respectively, for the five days of continuous operation of the experiment. Implying that under ideal conditions (without any foulant agent), the membranes can operate for long periods of time, maintaining a permeate flux and a rejection of salt at desired values. Additionally, the commercial membrane experienced a 21% flux decline (from 7.5 to 5.9 kg m^{-2} h^{-1}), while the OMT4 membrane experienced a 5% decline (from 8.0 to 7.6 kg m^{-2} h^{-1}).

In Fig. 7b, the performance of a commercial PVDF membrane and the OMT4 membrane was compared over a five-day fouling test using a feed solution containing 100 ppm of HA and 35 g L^{-1} of NaCl, where a pure crystalline water permeate was successfully obtained, as illustrated in Fig. S10.† The visual assessment (Fig. 8) shows that by day 3, the commercial PVDF membrane exhibited significant HA accumulation, with its surface nearly entirely covered by HA by the end of day 5. In contrast, the OMT4 membrane displayed considerably less fouling, with noticeable areas on its surface remaining free from HA accumulation throughout the test. This visual evidence underscores the superior antifouling properties of the OMT4 membrane compared to the commercial PVDF membrane. The results illustrated in Fig. 7b, revealed that the permeate flux began decreasing on the second day of operation, and the trend continued throughout the test. By the fourth day, the decrease in permeate flux was rapid, indicating the occurrence of scaling phenomena on the membrane surface. After the test, the commercial PVDF membrane exhibited a total decrease in permeate flux of 60%, while the OMT4 membrane experienced a decrease of 45%, showcasing superior performance. These findings suggest that the OMT4 membrane may be a more viable option than the commercial PVDF membrane.

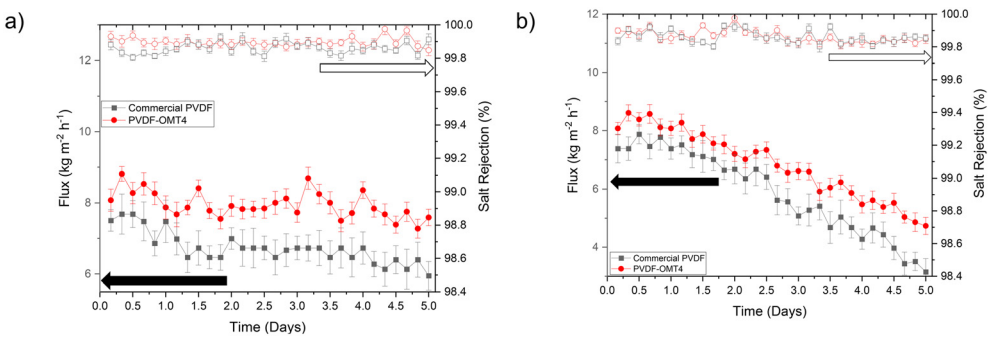

Fig. 7 Long-term stability test of commercial PVDF (black lines) and PVDF–OMT4 wt% (red lines) membranes for permeate flux and salt rejection in presence of only a) NaCl and b) NaCl with HA to promote scaling phenomena. Full and empty symbols represent the membrane flux (kg m^{-2} h^{-1}) and salt rejection (%), respectively. Error bars represent standard deviations from three samples (or five in the case of the porosity).

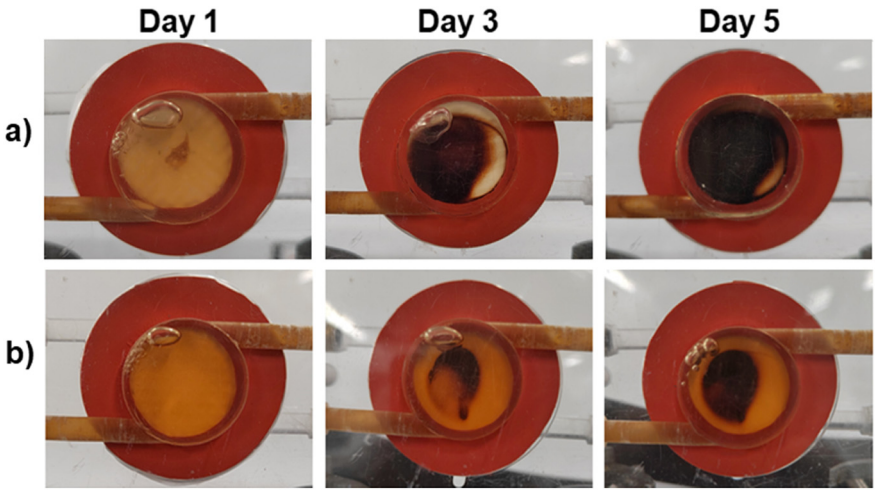

Fig. 8 Humic acid accumulation at the surface of the membrane after day 1, 3 and 5, for (a) commercial PVDF, and (b) OMT4 membranes (from top to bottom).

Table 1 Comparison of the performance of the fabricated membrane with that of a previously reported membrane in the literature

Ref.	MD type	Membrane type	Solution	Pore size (μm)	T_f (°C)	Permeate flux (kg m^{-2} h^{-1})
54	AGMD	PVDF (Millipore)	Artificial seawater	0.45	40–70	~1–7
55	AGMD	PTFE (Millipore)	NaCl (35 000 ppm)	0.20	5–45	0.5–6
56	VMD	Zeolite	NaCl (35 000 ppm)	0.07	60	5.2
57	AGMD	Clay-alumina	NaCl (30 000 ppm)	1.43	70	4.1
58	AGMD	Zr50	NaCl (50 000 ppm)	0.05	75	2.7
59	AGMD	Titania	NaCl (30 000 ppm)	—	90	3.7
60	AGMD	PTFE (Gore)	NaCl (35 000 ppm)	0.20	80	10.5
35	AGMD	GO-APTS	NaCl (35 000 ppm)	0.23	80	6.2
52	AGMD	PVDF-GO	NaCl (35 000 ppm)	0.49	75	10.7
This work	**AGMD**	**PVDF–OMT**	**NaCl (35 000 ppm)**	**0.21**	**60**	**8.6**

Table 1 displays the different experimental results reported in literature with different mixed matrix membranes, using different polymers and different filler materials. It can be observed that the results achieved in this work with PVDF–OMT membrane shows comparable performance to other membranes presented in Table 1, providing a permeate flux comparable with those reported by Alberto M. *et al.*,[52] who used graphene oxide as a filler. In our research, the permeate flux is slightly higher than those at 70 °C as showed in Fig. 6b, noting that the feed temperatures were lower by 5 °C, which could explain the difference in the obtained flux. The use of clays, in particular OMT, as filler material for water desalination, is highly promising, because of the high performance delivered and because their low-cost and readily availability. In contrast, other membranes mentioned in Table 1 were created using expensive materials such as zeolite, resulting in an expensive membrane synthesis process (70% of the cost is on the support).[53]

Fig. 9 shows a comparison between some commonly used fillers in MD. A radar chart was utilized to visualize five frequently used material fillers in membrane distillation based on key parameters, including permeate flux, contact angle, liquid entry pressure, pore wetting resistance, material cost, and availability. This method enables a comprehensive comparison, simplifying decision-making by considering technical performance along with practical and economic factors. The chart's customization options enable prioritisation based on specific application goals, making the material selection process more efficient. Please refer to Table S4 of the ESI† for a comprehensive understanding of the methodology utilized in this comparison, including the scoring matrix. As discussed earlier, the variables considered in this comparison are based on the fundamental characteristics that a material should possess for MD: permeate flux, contact angle, liquid entry pressure, pore wetting resistance, material cost and availability. A material may be cost-effective, but if it is scarce or subject to supply chain issues, it could pose a risk to continuous production. High availability ensures a stable and reliable material supply for consistent membrane fabrication. These selected materials, graphene oxide (GO), alumina, Cloisite 20A (OMT), titanium dioxide (TiO_2), and metal–organic frameworks (MOFs), are not only chosen for their unique properties but also for their common usage as membrane fillers in membrane distillation (MD) applications. Their prevalence in MD membranes stems from their distinct advantages, such as enhanced thermal conductivity (GO), chemical and thermal stability (alumina), hydrophobicity (OMT),

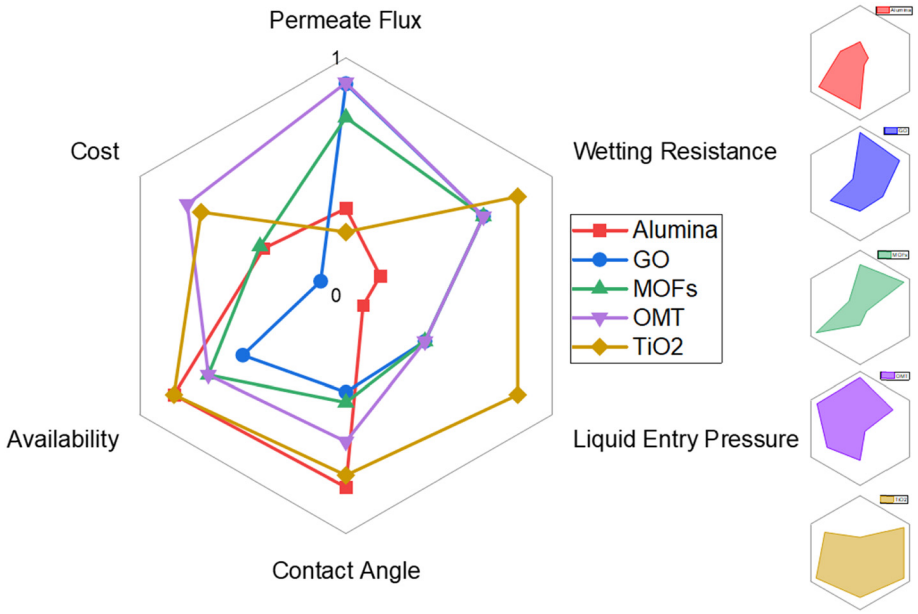

Fig. 9 Outline comparison of selected fillers used in membrane distillation.

photocatalytic properties for self-cleaning effects (TiO_2), and tunable characteristics with high porosity (MOFs). The radar chart will be a valuable tool to quantitatively assess and compare these commonly used materials, facilitating an informed decision-making process for selecting optimal membrane fillers in MD.

The comparison depicted in Fig. 9 is predicated on a scale that ranges from 0 to 1. As per the scale, values closer to 1 are preferable, and all the evaluation criteria carry equal weightage. On this basis, considering the parameter of permeate flux, two standout materials emerge as promising additives: OMT and GO. Both exhibit high permeate flux, making them particularly advantageous for applications prioritizing efficient vapour transport. On the contrary, TiO_2 demonstrates the lowest permeate flux among the materials considered. This lower flux might be attributed to specific inherent properties, suggesting that TiO_2 might be better suited for applications where high flux is not the primary concern. Moving on to LEP, TiO_2 stands out with the highest LEP, indicating more excellent resistance to liquid penetration. On the contrary, OMT and GO, while excelling in permeate flux, demonstrate moderate LEP, suggesting that these materials might be more permeable to liquid entry. Analysing the contact angle, TiO_2 and Alumina perform well, signifying high hydrophobicity. This property is valuable for preventing wetting and fouling in membrane distillation. OMT, with a good contact angle, also holds promise in this aspect. Considering cost-effectiveness, OMT emerges as a frontrunner with a relatively low cost. GO follows closely, presenting a good balance between cost and performance. TiO_2, despite its favourable characteristics, is also cost-effective, enhancing its overall appeal. Lastly, regarding availability, alumina and TiO_2 are noted as highly available materials, and MOFs and OMT follow closely. This availability and their respective properties enhance their practicality as potential membrane additives.

Based on the available data, OMT is a material that offers both cost-effectiveness and high performance on multiple indicators. Nevertheless, the optimal selection of a material should always consider the specific requirements of the intended application and the relative significance of each property.

The incorporation of clay nanoparticles, especially OMT, may increases the membrane's hydrophobicity and surface roughness.[46] This effectively prevents fouling and extends the membrane's operational lifespan. Additionally, this modification leads to a higher LEP, significantly improving the membrane's resistance to pore wetting and ensuring superior long-term performance. These advantageous properties highlight the potential of OMT-enhanced membranes for advanced membrane distillation applications.

Using phase inversion synthesis, PVDF–clay membrane were fabricated and used in membrane distillation for water treatment, presenting higher values of porosity, LEP, contact angle, small pore size, and long-term stability in the MD process than the others. Based on this, the PVDF–OMT membrane prepared in this work demonstrates competitive performance compared to those in Table 1 and Fig. 9.

4. Conclusions

Phase inversion synthesised PVDF membranes using DMSO as a non-toxic solvent were fabricated to be used in the AGMD system. A concentration of 18 wt% of PVDF in DMSO solution was found as the optimal membrane, showing better results in the membrane characteristics and permeate flux.

Clay materials have demonstrated a high degree of compatibility with PVDF polymer, rendering them suitable

for developing mixed-matrix membranes for membrane distillation. Through SEM-EDX analysis, the presence of clay materials on the membrane surface has been verified. The incorporation of small loadings (2, 4, 6 wt% based on polymer weight) of modified montmorillonite clay material into the PVDF membrane has resulted in a substantial increase in its structural properties, including LEP, contact angle, porosity, and pore size.

AGMD experiments were conducted using saline feed solution. The results showed that the PVDF–OMT (4 wt%) membrane had the highest permeate flux, measuring 8.6 kg m^{-2} h^{-1}, under a feed temperature of 60 °C. In comparison, the commercial and control PVDF membranes had permeate fluxes of 7.6 and 6.1 kg m^{-2} h^{-1}, respectively. These findings provide valuable insights into optimising membrane technology and improving its performance in various industrial applications.

PVDF–OMT membrane has shown its stability during the long-term MD process (120 hours of operation), maintaining a permeate flux of 8.1 kg m^{-2} h^{-1} and 99.8% of salt rejection. Still, work has to be done to improve the performance of the membrane against foulant agents in the feed solution. Humic acid was incorporated into the feed saline solution to induce organic fouling, in which experiment, the PVDF–OMT4 could maintain the permeate flux and salt rejection in desired values for 2.5 days, further that time reduction on the permeate flux was presented reaching a final reduction of 45%, that is better in comparison of the 60% permeate flux reduction presented by the commercial PVDF membrane.

The exceptional performance of the OMT4 membrane can be attributed to several key factors. Firstly, its significantly higher porosity of 87%, compared to 75% for the commercial PVDF membrane, which increases the available empty volume for vapour transport and reduces the diffusion path, thereby enhancing permeate flux. Additionally, the OMT4 membrane's improved pore size distribution, with a higher percentage of smaller pores, contributes to a better LEP of 4.6 bar, as opposed to 3.5 bar for the commercial PVDF membrane. This higher LEP indicates greater resistance to pore wetting, which is essential to ensure long-term performance. Furthermore, the combined effects of these properties result in a higher overall permeate flux of 8.6 kg m^{-2} h^{-1} for the OMT4 membrane, compared to 7.6 kg m^{-2} h^{-1} for the commercial counterpart. These findings demonstrate that the improved performance is not solely reliant on hydrophobicity but is also driven by the synergistic effects of enhanced porosity, defined pore size distribution, and increased LEP to enhance membrane's lifespan. Therefore, the OMT4 membrane presents a more effective solution for MD applications, showcasing the importance of considering multiple factors in membrane design and performance evaluation.

In conclusion, the integration of clay material onto the PVDF membranes has demonstrated a significant improvement in both the structural characteristics and efficiency of the membranes during the membrane distillation process.

Data availability

With this statement, the authors confirm that the data that support the findings of this study are available from the corresponding author upon a reasonable request.

Author contributions

Roberto Navarro-Tovar: writing – review & editing, writing – original draft, visualisation, methodology, investigation, formal analysis, conceptualisation. Megan Jobson: writing – review & editing, supervision, resources. Patricia Gorgojo: writing – review & editing, supervision, resources. Peter Martin: writing – review & editing, supervision, resources. Maria Perez-Page: writing – review & editing, validation, supervision, resources, project administration, methodology, investigation, funding acquisition, formal analysis, conceptualisation.

Conflicts of interest

The authors declare that they have no conflict of interest.

Acknowledgements

This work has been financially supported by the UK Research Council EPRSC with the Program Grant SynHiSel EP/V047078/1. Navarro-Tovar R. thank the Mexican National Council of Humanities, Sciences and Technologies CONAHCyT for its financial support through project No. 773949.

References

1 I. Tournis, D. Tsiourvas, Z. Sideratou, L. G. Boutsika, A. Papavasiliou, N. K. Boukos and A. A. Sapalidis, Superhydrophobic nanoparticle-coated PVDF–HFP membranes with enhanced flux, anti-fouling and anti-wetting performance for direct contact membrane distillation-based desalination, *Environ. Sci.: Water Res. Technol.*, 2022, **8**, 2373–2380.

2 M. Gryta, K. Karakulski and A. W. Morawski, Purification of oily wastewater by hybrid UF/MD, *Water Res.*, 2001, **35**, 3665–3669.

3 P. López-Porfiri, S. Ramos-Paredes, P. Núñez and P. Gorgojo, Towards the technological maturity of membrane distillation: the MD module performance curve, *npj Clean Water*, 2023, **6**, 18.

4 I. A. Said, N. Fuentes, Z. He, R. Xin, K. Zuo, W. S. Walker and Q. Li, Treatment of brackish water reverse osmosis brine using only solar energy, *Environ. Sci.: Water Res. Technol.*, 2021, **7**, 1840–1851.

5 I. A. Said, N. Fuentes, Z. He, R. Xin, K. Zuo and Q. Li, Low-cost desalination of seawater and hypersaline brine using nanophotonics enhanced solar energy membrane distillation, *Environ. Sci.: Water Res. Technol.*, 2020, **6**, 2180–2196.

6 V. R. Moreira, J. V. Raad, J. X. Lazarini, L. V. S. Santos and M. C. S. Amaral, Recent progress in membrane distillation

configurations powered by renewable energy sources and waste heat, *J. Water Process Eng.*, 2023, **53**, 103816.
7 Y. Choi, G. Naidu, L. D. Nghiem, S. Lee and S. Vigneswaran, Membrane distillation crystallization for brine mining and zero liquid discharge: opportunities, challenges, and recent progress, *Environ. Sci.: Water Res. Technol.*, 2019, **5**, 1202–1221.
8 J. Zhang, N. Li, D. Ng, I. A. Ike, Z. Xie and S. Gray, Depletion of VOC in wastewater by vacuum membrane distillation using a dual-layer membrane: mechanism of mass transfer and selectivity, *Environ. Sci.: Water Res. Technol.*, 2019, **5**, 119–130.
9 G. Zakrzewska-Trznadel, M. Harasimowicz and A. G. Chmielewski, Concentration of radioactive components in liquid low-level radioactive waste by membrane distillation, *J. Membr. Sci.*, 1999, **163**, 257–264.
10 N. A. S. Muhamad, N. Mokhtar, R. Naim, W. J. Lau and A. Ismail, A Review of Membrane Distillation Process: Before, During and After Testing, *Int. J. Eng. Technol. Sci.*, 2019, **6**, 62–81.
11 S. Kalla, S. Upadhyaya and K. Singh, Principles and advancements of air gap membrane distillation, *Rev. Chem. Eng.*, 2019, **35**, 817–859.
12 C. Skuse, A. Gallego-Schmid, A. Azapagic and P. Gorgojo, Can emerging membrane-based desalination technologies replace reverse osmosis?, *Desalination*, 2021, **500**, 114844.
13 J. Hao, L. Wang, X. Wang, J. Wang, M. He, X. Zhang, J. Wang, L. Nie and J. Li, Preparation, modification and antifouling properties of polyaniline conductive membranes for water treatment: a comprehensive review, *Environ. Sci.: Water Res. Technol.*, 2024, **10**, 105–127.
14 M. Li, Q. Zhao, S. Zhang, D. Li, H. Li, X. Zhang and B. Xing, Facile passivation of black phosphorus nanosheets via silica coating for stable and efficient solar desalination, *Environ. Sci.: Nano*, 2020, **7**, 414–423.
15 L. Ge, H. Song, J. Zhu, Y. Zhang, Z. Zhou and B. Van der Bruggen, Metal/covalent–organic framework based thin film nanocomposite membranes for advanced separations, *J. Mater. Chem. A*, 2024, **12**(14), 7975–8013.
16 J. Wang, Y. Qu, T. Liang, Z. Liu, P. Sun, Z. Li, X. Wang, Y. Hu, L. Wang and N. Wang, Fabrication of a graphene oxide-embedded separation bilayer composite nanofiltration membrane using a combination of layer-by-layer self-assembly and interfacial polymerization, *Environ. Sci.: Water Res. Technol.*, 2022, **8**, 1923–1937.
17 R. Leyva-Ramos, A. Jacobo-Azuara and J. I. Martínez-Costa, in *Porous Materials: Theory and Its Application for Environmental Remediation*, ed. J. C. Moreno-Piraján, L. Giraldo-Gutierrez and F. Gómez-Granados, Springer International Publishing, Cham, 2021, pp. 341–363.
18 P. Anadão, L. F. Sato, H. Wiebeck and F. R. Valenzuela-Díaz, Montmorillonite as a component of polysulfone nanocomposite membranes, *Appl. Clay Sci.*, 2010, **48**, 127–132.
19 H. Rajabi, N. Ghaemi, S. S. Madaeni, P. Daraei, M. A. Khadivi and M. Falsafi, Nanoclay embedded mixed matrix PVDF nanocomposite membrane: Preparation, characterization and biofouling resistance, *Appl. Surf. Sci.*, 2014, **313**, 207–214.
20 C. Y. Lai, A. Groth, S. Gray and M. Duke, Preparation and characterization of poly(vinylidene fluoride)/nanoclay nanocomposite flat sheet membranes for abrasion resistance, *Water Res.*, 2014, **57**, 56–66.
21 B. S. Kumar, A. Dhakshinamoorthy and K. Pitchumani, K10 montmorillonite clays as environmentally benign catalysts for organic reactions, *Catal. Sci. Technol.*, 2014, **4**, 2378–2396.
22 J. Zhu, X. Liu, M. L. Geier, J. J. McMorrow, D. Jariwala, M. E. Beck, W. Huang, T. J. Marks and M. C. Hersam, Layer-by-Layer Assembled 2D Montmorillonite Dielectrics for Solution-Processed Electronics, *Adv. Mater.*, 2016, **28**, 63–68.
23 Y. Zhou, H. Ding, A. T. Smith, X. Jia, S. Chen, L. Liu, S. E. Chavez, Z. Hou, J. Liu, H. Cheng, Q. Liu and L. Sun, Nanofluidic energy conversion and molecular separation through highly stable clay-based membranes, *J. Mater. Chem. A*, 2019, **7**, 14089–14096.
24 Z. Qiao, S. Zhao, J. Wang, S. Wang, Z. Wang and M. D. Guiver, A Highly Permeable Aligned Montmorillonite Mixed-Matrix Membrane for CO2 Separation, *Angew. Chem., Int. Ed.*, 2016, **55**, 9321–9325.
25 M.-Y. Huang, Y. Chen, X. Yan, X.-J. Guo, L. Dong and W.-Z. Lang, Two-dimensional Montmorillonite membranes with efficient water filtration, *J. Membr. Sci.*, 2020, **614**, 118540.
26 Z. Yang, Z. Yuan, Z. Shang and S. Ye, Multi-functional membrane based on montmorillonite/graphene oxide nanocomposites with high actuating performance and wastewater purification, *Appl. Clay Sci.*, 2020, **197**, 105781.
27 T. Zhang, B. Ren, H. Bai, T. Wen, L. Chen, S. Ma, X. Wang, S. Wang and Y. Zhao, Subnanometer-scale control of channel height in two-dimensional montmorillonite membrane for ion separation, *J. Membr. Sci.*, 2023, **675**, 121573.
28 S. Leaper, E. O. Avendaño Cáceres, J. M. Luque-Alled, S. H. Cartmell and P. Gorgojo, POSS-Functionalized Graphene Oxide/PVDF Electrospun Membranes for Complete Arsenic Removal Using Membrane Distillation, *ACS Appl. Polym. Mater.*, 2021, **3**, 1854–1865.
29 N. C. f. B. I. PubChem, PubChem Compound Summary for CID 702, Ethanol, **https://pubchem.ncbi.nlm.nih.gov/compound/Ethanol**, (accessed March 6, 2024).
30 J. M. Luque-Alled, S. Leaper, A. Abdel-Karim, C. Skuse and P. Gorgojo, PVDF membranes containing alkyl and perfluoroalkyl-functionalized graphene nanosheets for improved membrane distillation, *J. Environ. Chem. Eng.*, 2023, **11**, 109898.
31 B. S. Chemicals, Cloisite 20A Microgranulated Clay, **https://www.byk.com/en/products/additive-guide/cloisite-20-a**, (accessed 04/07/2023, 2023).
32 N. M. Mokhtar, W. J. Lau, A. F. Ismail and B. C. Ng, Physicochemical study of polyvinylidene fluoride–Cloisite15A® composite membranes for membrane distillation application, *RSC Adv.*, 2014, **4**, 63367–63379.

33 M. Rezaei, A. F. Ismail, S. A. Hashemifard and T. Matsuura, Preparation and characterization of PVDF-montmorillonite mixed matrix hollow fiber membrane for gas–liquid contacting process, *Chem. Eng. Res. Des.*, 2014, **92**, 2449–2460.

34 T. A. Geleta, I. V. Maggay, Y. Chang and A. Venault, Recent Advances on the Fabrication of Antifouling Phase-Inversion Membranes by Physical Blending Modification Method, *Membranes*, 2023, **13**(1), 1–53.

35 S. Leaper, A. Abdel-Karim, B. Faki, J. M. Luque-Alled, M. Alberto, A. Vijayaraghavan, S. M. Holmes, G. Szekely, M. I. Badawy, N. Shokri and P. Gorgojo, Flux-enhanced PVDF mixed matrix membranes incorporating APTS-functionalized graphene oxide for membrane distillation, *J. Membr. Sci.*, 2018, **554**, 309–323.

36 A. Abdel-Karim, J. M. Luque-Alled, S. Leaper, M. Alberto, X. Fan, A. Vijayaraghavan, T. A. Gad-Allah, A. S. El-Kalliny, G. Szekely, S. I. A. Ahmed, S. M. Holmes and P. Gorgojo, PVDF membranes containing reduced graphene oxide: Effect of degree of reduction on membrane distillation performance, *Desalination*, 2019, **452**, 196–207.

37 P. Moradihamedani, Recent development in polymer/montmorillonite clay mixed matrix membranes for gas separation: a short review, *Polym. Bull.*, 2023, **80**, 4663–4687.

38 A. Alkhudhiri, N. Darwish and N. Hilal, Membrane distillation: A comprehensive review, *Desalination*, 2012, **287**, 2–18.

39 V. Calabro, B. L. Jiao and E. Drioli, Theoretical and Experimental Study on Membrane Distillation in the Concentration of Orange Juice, *Ind. Eng. Chem. Res.*, 1994, **33**, 1803–1808.

40 J. E. Marshall, A. Zhenova, S. Roberts, T. Petchey, P. Zhu, C. E. J. Dancer, C. R. McElroy, E. Kendrick and V. Goodship, On the Solubility and Stability of Polyvinylidene Fluoride, *Polymers*, 2021, **13**(9), 1–31.

41 A. Karimi, A. Khataee, V. Vatanpour and M. Safarpour, The effect of different solvents on the morphology and performance of the ZIF-8 modified PVDF ultrafiltration membranes, *Sep. Purif. Technol.*, 2020, **253**, 117548.

42 C. Alexowsky, M. Bojarska and M. Ulbricht, Porous poly(vinylidene fluoride) membranes with tailored properties by fast and scalable non-solvent vapor induced phase separation, *J. Membr. Sci.*, 2019, **577**, 69–78.

43 D. Matveev, I. Borisov, V. Vasilevsky, G. Karpacheva and V. Volkov, Spinning of Polysulfone Hollow Fiber Membranes Using Constant Dope Solution Composition: Viscosity Control via Temperature, *Membranes*, 2022, **12**(12), 1–16.

44 S. Zhang, L. Shen, H. Deng, Q. Liu, X. You, J. Yuan, Z. Jiang and S. Zhang, Ultrathin Membranes for Separations: A New Era Driven by Advanced Nanotechnology, *Adv. Mater.*, 2022, **34**, 2108457.

45 Y. Liao, R. Wang, M. Tian, C. Qiu and A. G. Fane, Fabrication of polyvinylidene fluoride (PVDF) nanofiber membranes by electro-spinning for direct contact membrane distillation, *J. Membr. Sci.*, 2013, **425–426**, 30–39.

46 P. Daraei and N. Ghaemi, Synergistic effect of Cloisite 15A and 30B nanofillers on the characteristics of nanocomposite polyethersulfone membrane, *Appl. Clay Sci.*, 2019, **172**, 96–105.

47 A. B. D. Cassie and S. Baxter, Wettability of porous surfaces, *Trans. Faraday Soc.*, 1944, **40**, 546–551.

48 J. A. Sanmartino, M. Khayet and M. C. García-Payo, in *Emerging Membrane Technology for Sustainable Water Treatment*, ed. N. P. Hankins and R. Singh, Elsevier, Boston, 2016, pp. 77–109.

49 S. Zhou, Z. Han, X. Wang, X. Liu, H. Hao, J. Xing, J. Dong, H. Liu and L. Liao, Low-cost and high-safety montmorillonite-based solid electrolyte for lithium metal batteries, *Appl. Clay Sci.*, 2024, **251**, 107329.

50 S. Lin, N. Y. Yip and M. Elimelech, Direct contact membrane distillation with heat recovery: Thermodynamic insights from module scale modeling, *J. Membr. Sci.*, 2014, **453**, 498–515.

51 L. D. Tijing, Y. C. Woo, J.-S. Choi, S. Lee, S.-H. Kim and H. K. Shon, Fouling and its control in membrane distillation—A review, *J. Membr. Sci.*, 2015, **475**, 215–244.

52 M. Alberto, C. Skuse, M. Tamaddondar and P. Gorgojo, Immobilized graphene oxide-based membranes for improved pore wetting resistance in membrane distillation, *Desalination*, 2022, **537**, 115898.

53 Y. Morigami, M. Kondo, J. Abe, H. Kita and K. Okamoto, The first large-scale pervaporation plant using tubular-type module with zeolite NaA membrane, *Sep. Purif. Technol.*, 2001, **25**, 251–260.

54 F. A. Banat and J. Simandl, Desalination by Membrane Distillation: A Parametric Study, *Sep. Sci. Technol.*, 1998, **33**, 201–226.

55 S. T. Hsu, K. T. Cheng and J. S. Chiou, Seawater desalination by direct contact membrane distillation, *Desalination*, 2002, **143**, 279–287.

56 A. Garofalo, M. C. Carnevale, L. Donato, E. Drioli, O. Alharbi, S. A. Aljlil, A. Criscuoli and C. Algieri, Scale-up of MFI zeolite membranes for desalination by vacuum membrane distillation, *Desalination*, 2016, **397**, 205–212.

57 R. Das, K. Sondhi, S. Majumdar and S. Sarkar, Development of hydrophobic clay–alumina based capillary membrane for desalination of brine by membrane distillation, *J. Asian Ceram. Soc.*, 2016, **4**, 243–251.

58 S. Cerneaux, I. Strużyńska, W. M. Kujawski, M. Persin and A. Larbot, Comparison of various membrane distillation methods for desalination using hydrophobic ceramic membranes, *J. Membr. Sci.*, 2009, **337**, 55–60.

59 J. Kujawa, S. Cerneaux and W. Kujawski, Investigation of the stability of metal oxide powders and ceramic membranes grafted by perfluoroalkylsilanes, *Colloids Surf., A*, 2014, **443**, 109–117.

60 A. Cipollina, M. G. Di Sparti, A. Tamburini and G. Micale, Development of a Membrane Distillation module for solar energy seawater desalination, *Chem. Eng. Res. Des.*, 2012, **90**, 2101–2121.